Morphological, Structural, and Chemical Effects in Response of Novel Carbide Derived Carbon Sensor to NH_3, N_2O, and Air

Kofi W. Adu,[†,‡,▽] Qixiu Li,[†,§] Sharvil C. Desai,[||] Anton N. Sidorov,[||] Gamini U. Sumanasekera,[||,⊥] and Angela D. Lueking*[,†,§]

Materials Research Laboratory, Pennsylvania State University, University Park, Pennsylvania 16802, Department of Energy and Mineral Engineering, Pennsylvania State University, University Park, Pennsylvania 16802, Department of Electrical and Computer Engineering, University of Louisville, Kentucky 40292, and Department of Physics, University of Louisville, Kentucky 40292

Received February 12, 2008. Revised Manuscript Received August 19, 2008

The response of two carbide derived carbons (CDCs) films to NH_3, N_2O, and room air is investigated by four probe resistance at room temperature and pressures up to 760 Torr. The two CDC films were synthesized at 600 (CDC-600) and 1000 °C (CDC-1000) to vary the carbon morphology from completely amorphous to more ordered, and determine the role of structure, surface area, and porosity on sensor response. Sensor response time followed kinetic diameter and indicated a more ordered carbon structure slowed response due to increased tortuosity caused by the formation of graphitic layers at the particle fringe. Steady state sensor response was greater for the less-ordered material, despite its decreased surface area, decreased micropore volume, and less favorable surface chemistry, suggesting carbon structure is a stronger predictor of sensor response than surface chemistry. The lack of correlation between adsorption of the probe gases and sensor response suggests chemical interaction (charge transfer) drive sensor response within the material; N_2O response, in particular, did not follow simple adsorption behavior. Based on Raman and FTIR characterization, carbon morphology (disorder) appeared to be the determining factor in overall sensor response, likely due to increased charge transfer between gases and carbon defects of amorphous or disordered regions. The response of the amorphous CDC-600 film to NH_3 was 45% without prior oxidation, showing amorphous CDCs have promise as chemical sensors without additional pretreatment common to other carbon sensors.

Introduction

A major goal in chemical sensor research is to develop a device that acts as an "electronic nose", differentiating between chemicals by providing different (or traceable) responses to different gaseous species in a complex mixture. For many applications, a desirable sensor property would be room temperature operation such that heating would not be required for monitoring ambient conditions. Room temperature operation would allow identification of organic species without thermal degradation and safe monitoring of combustible gases. Room temperature gas sensing has been demonstrated for carbon materials, including carbon nanotubes (CNTs),[1−7] conducting polymers,[8] and composites of conducting carbon black with polymers[9−13] or organic molecules.[14] Although CNT and polymer-based sensors provide advantages by operating at room temperature, their operation may be subject to long-term drift, a nonlinear response, and the requirement of significant heating to regain performance after exposure to high analyte concentrations. The latter is due to the strength of the gas−solid interaction. NH_3 adsorption on CNTs, for example, may be due to a combination of chemical and physical adsorption;[15] thus using a carbon-based sensor for detection of NH_3 generally requires heating the sensor to elevated temperature after gas exposure. It has been shown theoretically that the sensitivity of CNT based sensors is due to partial charge transfer between the analyte and the CNT even at room temperature.[16]

For CNTs, Kong et al. demonstrated a 100 fold change in the electrical conductivity of individual single-walled nanotube (SWNT) upon exposure to 2−200 ppm of NO_2, and a three-orders of magnitude change upon exposure to 0.1−1% of NH_3 in Ar.[5] Subsequent work with multiwalled carbon nanotubes (MWNTs) indicated a tractable electrical response upon gas exposure,[6] providing the potential for a significant cost decrease in the fabrication of CNT based sensors. Later work with CNT based sensors indicated the morphological features and structure

* To whom correspondence should be addressed. E-mail: leuking@psu.edu.
[†] Materials Research Laboratory, Pennsylvania State University.
[‡] Department of Physics, Pennsylvania State University.
[§] Department of Energy and Mineral Engineering, Pennsylvania State University.
[||] Department of Electrical and Computer Engineering, University of Louisville.
[⊥] Department of Physics, University of Louisville.
[▽] Current Address: YTC America, Inc., Camarillo, CA 93012.

(1) Wang, S. G.; Zhang, Q.; Yang, D. J.; Sellin, P. J.; Zhong, G. F. *Diamond Relat. Mater.* **2004**, *13*, 1327–1332.
(2) Quang, N. H.; Van Trinh, M.; Lee, B. H.; Huh, J. S. *Sens. Actuators, B* **2006**, *113*, 341–346.
(3) Arab, M.; Berger, F.; Picaud, F.; Ramseyer, C.; Glory, J.; Mayne-L'Hermite, M. *Chem. Phys. Lett.* **2006**, *433*, 175–181.
(4) Feng, X.; Irle, S.; Witek, H.; Morokuma, K.; Vidic, R.; Borguet, E. *J. Am. Chem. Soc.* **2005**, *127*, 10533–10538.
(5) Kong, J.; Franklin, N. R.; Zhou, C. W.; Chapline, M. G.; Peng, S.; Cho, K. J.; Dai, H. J. *Science* **2000**, *287*, 622–625.
(6) Varghese, O. K.; Kichambre, P. D.; Gong, D.; Ong, K. G.; Dickey, E. C.; Grimes, C. A. *Sens. Actuators, B* **2001**, *81*, 32–41.
(7) Nguyen, H. Q.; Huh, J. S. *Sens. Actuators, B* **2006**, *117*, 426–430.
(8) Barisci, J. N.; Lewis, T. W.; Spinks, G. M.; Too, C. O.; Wallace, G. G. *J. Intell. Mater. Syst. Struct.* **1998**, *9*, 723–731.
(9) Sisk, B. C.; Lewis, N. S. *Langmuir* **2006**, *22*, 7928–7935.
(10) Li, J. R.; Xu, J. R.; Zhang, M. Q.; Rong, M. Z. *Carbon* **2003**, *41*, 2353–2360.
(11) Dong, X. M.; Fu, R. W.; Zhang, M. Q.; Zhang, B.; Rong, M. Z. *Carbon* **2004**, *42*, 2551–2559.
(12) Zhang, B.; Fu, R. W.; Zhang, M. Q.; Dong, X. M.; Wang, L. C.; Pittman, C. U. *Mater. Res. Bull.* **2006**, *41*, 553–562.
(13) Dong, X. M.; Fu, R. W.; Zhang, M. Q.; Zhang, B.; Li, J. R.; Rong, M. Z. *Polym. Bull.* **2003**, *50*, 99–106.
(14) Gao, T.; Woodka, M. D.; Brunschwig, B. S.; Lewis, N. S. *Chem. Mater.* **2006**, *18*, 5193–5202.
(15) Stoeckli, F.; Guillot, A.; Slasli, A. M. *Carbon* **2004**, *42*, 1619–1624.
(16) Zhao, J. J.; Buldum, A.; Han, J.; Lu, J. P. *Nanotechnology* **2002**, *13*, 195–200.

10.1021/la800465e CCC: $40.75
Published on Web 11/24/2008

of the CNT played key role in the sensor response, including (1) the nature of the carbon bonding and the number of graphitic particles,[17] the number of conducting electrons,[18,19] and defects[19] within the carbon structure, (2) the surface functionalities present on the surface either due to synthesis or oxidative pretreatment,[4,7] and (3) possible swelling of micropores upon gas adsorption.[20] In general, the morphological features (point 1) of CNT are difficult to control, particularly when synthesized in large-scale where low yield may lead to the presence of significant amounts of graphitic particles that affect sensor performance. The effect of surface functionality (point 2) may change with increasing air exposure; and aging effects on sensor performance have been noted.[21] These points may explain, in part, the variation in reported values of CNT sensor response. For example, the sensitivity of MWNT to NH_3 at room temperature varies from 5−13%[2,3] to as high as 60%.[1,6] However, in the latter case, it appears the large response may be due in part to an interaction between the MWNT and the sensor support.

Recent work in CNT sensor development includes doping CNTs with metals to increase the selectivity.[22,23] Incorporating metals and metal oxides into CNT sensors exploit the inherent sensing properties of the metal (or metal oxide) dopant, while dispersing and stabilizing the dopant to increase the surface-to volume ratio (hence the sensing properties) of the nanosized metal (or metal oxide) particles. The metal (metal oxide) improves not only the selectivity of the CNT-based gas sensor, but enhances the sensitivity and the response time as well. For example, in hydrogen sensing, group VIII transition metals like Ni, Pt and Pd are mostly used due to the high affinity of the metal toward hydrogen, which changes the properties of the metal due to the formation of the metal hydride.[24]

The use of other carbon materials, such as activated carbon and/or graphite derivatives, as chemical sensors (without added metal) is very limited. Amorphous carbon black (CB) has been added to nonconducting polymers[9−13] to serve as the conducting media for resistive sensing of organic vapors. In these studies, the sensing mechanism is quite different from the CNT sensing studies described above as the CB/polymer matrix is for vapor sensing (rather than gas sensing of CNTs), and CB is generally considered inert, as absorption occurs to the polymeric[9−13] or organic[14] phase. Within the CB/polymer matrix, swelling of the polymeric/organic phase disrupts the connectivity of the carbon black, leading to a tractable response to the analyte.[9] The electric resistance has been found to correlate to adsorption, and has been related to Freundlich adsorption isotherms.[11] Decreasing the carbon black fraction of the composite increases sensitivity, but leads to a nonlinear sensor response.[9]

The structure of carbide-derived-carbons (CDCs), recently developed by Gogotsi et al.,[25−30] is dependent upon the metal carbide precursor and the temperature of metal abstraction. At high preparation temperatures, the CDCs become more ordered, and may bear resemblance to carbon black. CDCs may also contain nanographene ribbons,[31,32] and thus bear a certain resemblance to CNTs. Unlike CNTs or carbon black, CDCs have a tightly controlled micropore structure that has shown superior performance in gas storage[29,33] and electrochemical capacitance[34,35] applications. The control of the tunable CDC pore size may allow control of sensor response, as porosity is related to gas adsorption.[29,33] To the best of our knowledge, there is no published work involving CDCs as chemical sensors and the objective of this work was to explore the sensitivity of CDC-based sensors to various gases. Here, we explore the room temperature resistive response of B_4C-derived CDCs to NH_3, N_2O and ambient air at pressures up to 760 Torr. Preparation temperature has a moderate effect on pore size distribution (PSD) and specific surface area (SSA) for B_4C-derived CDCs.[26] At low temperature (i.e., 600 °C), B_4C can be completely extracted, but XRD indicates the resulting carbon is completely amorphous. At moderate temperatures (i.e., 800−1000 °C), SSA is increased without sacrificing micropore volume, and graphitic layers start to form as the material becomes more ordered. At higher temperatures (i.e., 1200 °C), SSA and microporosity begins to decrease as the carbon further aligns to form graphite. Our results show a high potential of using the CDC as gas sensors.

Experimental Details

The basic procedure for CDC synthesis has been described previously by Gogotsi et al.,[25] whereby variations in chlorine extraction conditions (time and temperature) led to variations in pore size, pore volume and SSA. In brief, CDCs are synthesized via metal abstraction with Cl_2 from a metal carbide precursor[25] at elevated temperatures, typically ranging from 600 to 1200 °C. In this work, 3 g of B_4C powder (Alfa Aesar, 99.4%, 1−7 μm) was treated at 600 and 1000 °C in a vertical furnace. In our laboratory, we have noted that carbides extracted at the same reaction conditions lead to CDC products with surface area and porosity that is within the experimental error of the measurement. The vertical mounting position promotes effective and uniform metal abstraction due to gas flow through the bed. The system was purged with Argon for one hour and then heated to 600 at 10 °C/min under argon flow. At 600 °C the flow gas was switched to chlorine gas (Cl_2) for 9 h, after which the system was cooled down to room temperature under Argon flow. Another sample was prepared at 1000 °C with 3 h Cl_2 dwell time. The two samples prepared by this process at 600 and 1000 °C will henceforth be referred to as CDC-600 and CDC-1000, respectively.

Raman spectra were collected at room temperature in the backscattering configuration using Renishaw inVia spectrometer

(17) Cantalini, C.; Valentini, L.; Lozzi, L.; Armentano, I.; Kenny, J. M.; Santucci, S. *Sens. Actuators, B* **2003**, *93*, 333–337.
(18) Valentini, L.; Mercuri, F.; Armentano, I.; Cantalini, C.; Picozzi, S.; Lozzi, L.; Santucci, S.; Sgamellotti, A.; Kenny, J. M. *Chem. Phys. Lett.* **2004**, *387*, 356–361.
(19) Kombarakkaran, J.; Clewett, C. F. M.; Pietrass, T. *Chem. Phys. Lett.* **2007**, *441*, 282–285.
(20) Kobayashi, N.; Enoki, T.; Ishii, C.; Kaneko, K.; Endo, M. *J. Chem. Phys.* **1998**, *109*, 1983–1990.
(21) Sayago, I.; E., T.; Aleixandre, M.; Horrillo, M. C.; Fernandez, M. J.; Lozano, J.; Lafuente, E.; Maser, W. K.; Benito, A. M.; Martinez, M. T.; Gutierrez, J.; Munoz, E. *Sens. Actuators, B* **2007**, *122*, 75–80.
(22) Star, A.; Joshi, V.; Skarupo, S.; Thomas, D.; Gabriel, J.-C. P. *J. Phys. Chem. B* **2006**, *110*, 21014–21020.
(23) Espinosa, E. H.; Ionescu, R.; Llobet, E.; Felten, A.; Bittencourt, C.; Sotter, E.; Topalian, Z.; Heszler, P.; Granqvist, C. G.; Pireaux, J. J.; Correig, X. *J. Electrochem. Soc.* **2007**, *154*, J141-J149.
(24) Drake, C.; Deshpande, S.; Bera, D.; Seal, S. *Int. Mater. Rev.* **2007**, *52*, 289–317.
(25) Gogotsi, Y.; Nikitin, A.; Ye, H. H.; Zhou, W.; Fischer, J. E.; Bo, Y.; Foley, H. C.; Barsoum, M. W. *Nat. Mater.* **2003**, *2*, 591–594.
(26) Dash, R. K.; Nikitin, A.; Gogotsi, Y. *Microporous Mesoporous Mater.* **2004**, *72*, 203–208.
(27) Erdemir, A.; Kovalchenko, A.; McNallan, M. J.; Welz, S.; Lee, A.; Gogotsi, Y.; Carroll, B. *Surf. Coat. Technol.* **2004**, *188−89*, 588–593.
(28) Dash, R. K.; Yushin, G.; Gogotsi, Y. *Microporous Mesoporous Mater.* **2005**, *86*, 50–57.
(29) Dash, R.; Chmiola, J.; Yushin, G.; Gogotsi, Y.; Laudisio, G.; Singer, J.; Fischer, J.; Kucheyev, S. *Carbon* **2006**, *44*, 2489–2497.
(30) Hoffman, E.; Yushin, G.; Gogotsi, Y.; Barsoum, M. *Abstr. Pap.-Am. Chem. Soc.* **2006**, 231.
(31) Yushin, G.; Dash, R.; Jagiello, J.; Fischer, J. E.; Gogotsi, Y. *Adv. Funct. Mater.* **2006**, *16*, 2288–2293.
(32) Hoffman, E. N.; Yushin, G.; Barsoum, M. W.; Gogotsi, Y. *Chem. Mater.* **2005**, *17*, 2317–2322.
(33) Gogotsi, Y.; Dash, R. K.; Yushin, G.; Yildirim, T.; Laudisio, G.; Fischer, J. E. *J. Am. Chem. Soc.* **2005**, *127*, 16006–16007.
(34) Chmiola, J.; Yushin, G.; Gogotsi, Y.; Portet, C.; Simon, P.; Taberna, P. L. *Science* **2006**, *313*, 1760–1763.
(35) Chmiola, J.; Yushin, G.; Dash, R.; Gogotsi, Y. *J. Power Sources* **2006**, *158*, 765–772.

equipped with a Peltier cooled RenCam dd-CCD. A Leica DM LM confocal microscope with 100× objective was used to illuminate the sample and collect the scattered light. It was set to operate at ~1 μm diameter focal spot size at the plane of the sample. A HeNe laser was used to excite the spectra, and the power at the sample was ~ 0.1mW measured using a miniature hand-held radiometer. The spectra were collected in air under ambient conditions using 633 nm radiation. Both H and V polarized light were accepted in the scattered radiation.

FTIR was collected using a BOMEM DA3+ FT spectrometer. The carbide material was first ultrasonicated in 2-propanol then deposited from solution onto ZnSe substrates maintained in air at 60 °C. The solvent from each drop was allowed to evaporate before the next drop was added to build up a carbide film. Prior to measurement, the film was heated at 100 °C for about 30 min, the sample was exposed to ambient air upon transfer to the FTIR chamber. The spectrum of the carbide film was obtained by removing the reflection/adsorption losses from the ZnSe substrate. The spectral resolution of IR measurements was 4 cm^{-1}.

The SSA of CDC-600 and CDC-1000 was determined using the BET equation with N_2 gas at 77 K (Micromeritics ASAP 2020). The samples were degassed at 300 °C under high vacuum ($P \approx 10^{-7}$ torr) for 12 h prior to measurements. To obtain pore volume and PSD, the density functional theory (DFT) model provided with the equipment with slit-geometry model option was used. Total pore volume was obtained at 95% of the saturation pressure. The total micropore volume was determined from the DFT analysis, considering pores less than 20 Å, and used the incremental surface area (ISA) as a function of pore width for the PSD. High resolution transmission electron microscopy, or HR-TEM (JEOL 2010F), was used to obtain morphological and structural information such as fringe and graphitic order of the CDC samples.

To prepare a thin uniform CDC film of 5 mm × 5 mm area, the CDC was first suspended in isopropyl alcohol (IPA) using Electrowave aqua-sonicator model EW-24tEXP operated at 40 °C for 30 min. The IPA-CDC suspension was drip coated onto a clean quartz substrate to form a thin film for the electrical measurements. The film was allowed to dry in air. Four passivated copper leads (all 0.003 in. diameter Wires from Omega) were attached to the edges of the 5 mm × 5 mm film with silver paste to measure the four probe electrical resistance. Prior to measurement, the system was first degassed at 100 °C in a 10^{-7} Torr vacuum for 6 h to cure the silver paste and remove any residual IPA. The resistance measurements were performed at room temperature in a standard van der Pauw configuration[36] via an integrated current source-DVM system (Keithley; model 2400). The four probe resistance measure geometry eliminates any contribution from silver paste and copper wire leads to the overall measured resistance. Such technique has been widely employed to interrogate the transport properties of carbon nanotubes.[37−41] The resistive response, $\Delta R/R_o = (R - R_o)/R_o$, was measured upon exposure to three gases: ambient air, N_2O and NH_3 (in that order), where R is the resistance at any time and R_o is the initial resistance of the film. The initial resistance R_o depended on the film thickness, however, the relative change in resistance ($\Delta R/R_o$) of different films from the same sample batch was independent of film thickness. The inlet pressure of the gas was systematically increased to 10, 50, 150, 250, 500, and 700 Torr. At each pressure step, both the resistance and the change in pressure were monitored. At the conclusion of each individual gas measurement, the system was degassed again at 10^{-7} Torr and 100 °C to recover the initial room temperature resistance. Several films of the same material were tested in this manner, and reported error bars represent one standard deviation of 2−3 measurements on different films of the same material. The change in pressure over the course of the experiment is proportional to the gas adsorbed on the sample. (The relation between pressure drop and moles adsorbed is the basis for the volumetric method of gas adsorption. In brief, the ideal gas equation, $PV = nRT$, demonstrates that at constant volume and temperature $\Delta P \propto \Delta n$). The adsorption plots are not true isotherms as equilibrium has not necessarily been reached even after the 10 min allowed at each pressure. In most carbon materials, longer times are generally allowed for gas adsorption to reach equilibrium, but the time is dependent upon the adsorbate−adsorbent pair, the initial concentration, the adsorption temperature, and the adsorption mechanism (i.e., physisorption vs chemisorption). For example, at low temperature (i.e., 40 °C) ammonia adsorption on activated carbon generally require 20−40 min for equilibrium to occur.[42]

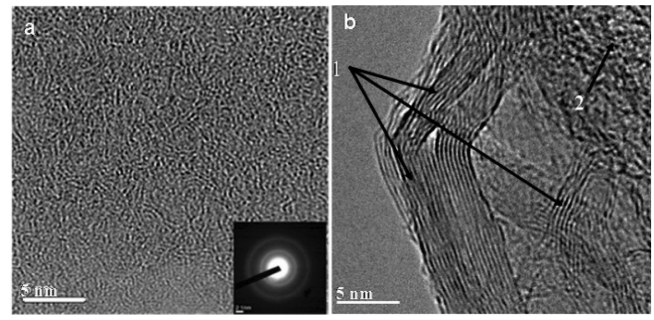

Figure 1. (a) HRTEM of CDC-600 shows the carbon structure is noncrystalline but with some texture. The insert SAD indicates the amorphous structure of the CDC. (b) HRTEM of CDC-1000 shows the presence of a mixture of graphitic layers of interplanar distance of 0.34 nm (arrows labeled 1) and a noncrystalline amorphous structure (arrow labeled 2).

Results

CDC Structure. The TEM of CDC-600 depicts a network structure with no order (Figure 1a). It is purely amorphous in nature as confirmed by the selected area diffraction (SAD inset, Figure 1a). In CDC-1000 graphitic layers with interplanar distance of ~0.34 nm ('1', in Figure 1b) have begun to appear at the edges of the material, but amorphous carbon ('2', Figure 1b) is still present. Raman spectrum of the B_4C precursor show distinct features, all below 1100 cm^{-1} (Figure 2); these features are completely absent in CDC-600 and CDC-1000. Instead, both CDC-600 and CDC-1000 have the "D" (disorder) and "G" (graphite) peaks characteristic of carbon materials at ~1320 and ~1590 cm^{-1}, respectively (Figure 2). The pronounced D peak is characteristic of highly disordered carbon for both materials. Increasing the preparation temperature from 600 to 1000 °C has decreased D:G: from 1.87 to 1.70 for CDC-600 and CDC-1000, respectively, showing the disorder decreases slightly with increased preparation temperature. The location of the G-peak, at frequencies above 1580 cm^{-1} has been associated with 'chain-like' sp^2 carbon.[43,44] Thus, the higher preparation temperature of CDC-1000 provides a modest increase in carbon order relative to CDC-600, and the increase in G peak frequency is an indication that sp^2 is more aligned in chain-like carbon structures for CDC-1000.

Surface Area and Porosity. The BET SSA and the total pore volume measured for CDC-1000 are 1286 and 0.5178 cm^2/g, respectively, compared to 978 and 0.4343 cm^2/g for CDC-600

(36) Van der Pauw, L. J. *Philips Res. Rep.* **1958**, *13*, 1–9.
(37) Sumanasekera, G. U.; Pradhan, B. K.; Romero, H. E.; Adu, K. W.; Eklund, P. C. *Phys. Rev. Lett.* **2002**, 89.
(38) Sumanasekera, G. U.; Pradhan, B. K.; Adu, C. K. W.; Romero, H.; Eklund, P. C. *Abstr. Pap. Am. Chem. Soc.* **2004**, *228*, U681–U681.
(39) Sumanasekera, G. U.; Pradhan, B. K.; Adu, C. K. W.; Romero, H. E.; Foley, H. C.; Eklund, P. C. *Mol. Cryst. Liq. Cryst.* **2002**, *387*, 255–261.
(40) Adu, C. K. W.; Sumanasekera, G. U.; Pradhan, B. K.; Romero, H. E.; Eklund, P. C. *Chem. Phys. Lett.* **2001**, *337*, 31–35.
(41) Sumanasekera, G. U.; Adu, C. K. W.; Fang, S.; Eklund, P. C. *Phys. Rev. Lett.* **2000**, *85*, 1096–1099.
(42) Rodrigues, C. C.; de Moraes, D.; da Nobrega, S. W.; Barboza, M. G. *Bioresour. Technol.* **2007**, *98*, 886–891.
(43) Ferrari, A. C.; Robertson, J. *Phys. Rev. B* **2001**, *64*, 075414.
(44) Ferrari, A. C.; Robertson, J. *Phys. Rev. B* **2000**, *61*, 14095–14107.

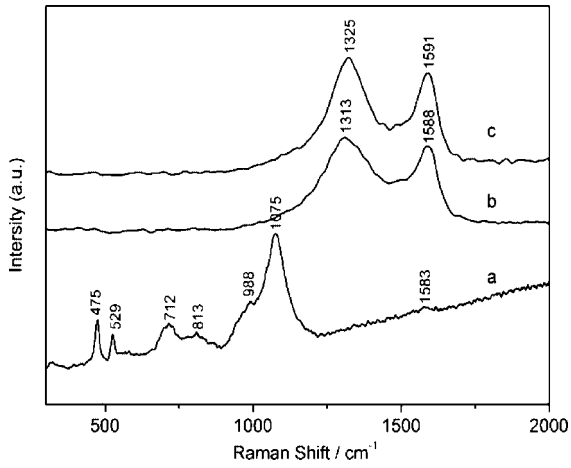

Figure 2. Raman spectra for (a) the B_4C precursor, (b) CDC-600, and (c) CDC-1000. The D:G ratios (based on peak area) are 1.87 and 1.70 for (b) and (c), respectively.

Table 1. BET Surface Area and Total Volume of Pores of CDC-600 and CDC-1000

sample	BET surface area (m^2/g)	micropore volume (cm^3/g)	total pore volume (cm^3/g)
CDC-1000	1287.0	0.41	0.52
CDC-600	978.2	0.30	0.43

(Table 1). Expected to dominate in the adsorptive gas response, the micropore volume is 0.41 cm^3/g for CDC-1000 and 0.30 cm^3/g for CDC-600 (Table 1). Thus, a significant microporosity remains in our material despite using pure Cl_2 in the extraction process. (High Cl_2 concentration may lead to carbon etching and large pores as observed in zirconium carbide-derived CDCs.[28]) The PSD of CDC-600 and CDC-1000 are qualitatively similar, yet CDC-1000 has a greater area attributable to pores of width between ~0.5 and ~0.8 nm (Figure 3). However, the width of the 0.5 nm peak in the PSD is broader for CDC-600, with CDC-600 having greater SSA in the range of ~0.6 nm to just below 2 nm (Figure 3, inset). CDC-1000 has greater pore area for pores greater than 2 nm (see Figure 3 inset). The results are consistent with previous studies for B_4C-derived CDCs,[26] in which moderate increase in preparation temperature (from 600 to ~900 °C) led to increase in micorpore volume, whereas high preparation temperature (i.e., 1200 °C) led to coalescence of micropores to form mesopores.

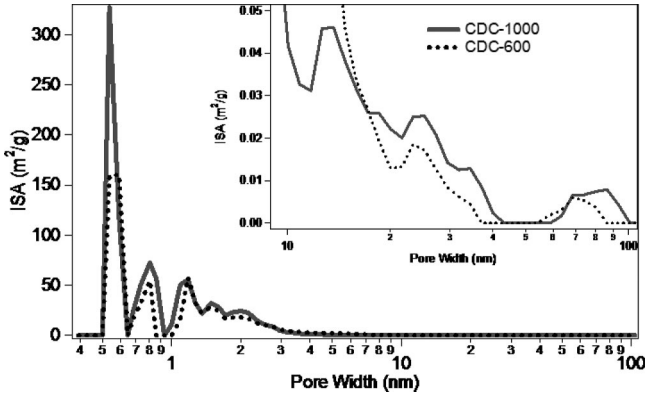

Figure 3. Pore size distribution, calculated from N_2 adsorption for CDC-600 (dashed line) and CDC-1000 (solid line) shows preparation conditions alter the pore structure. The inset is a zoom of the macropore and mesopore regions.

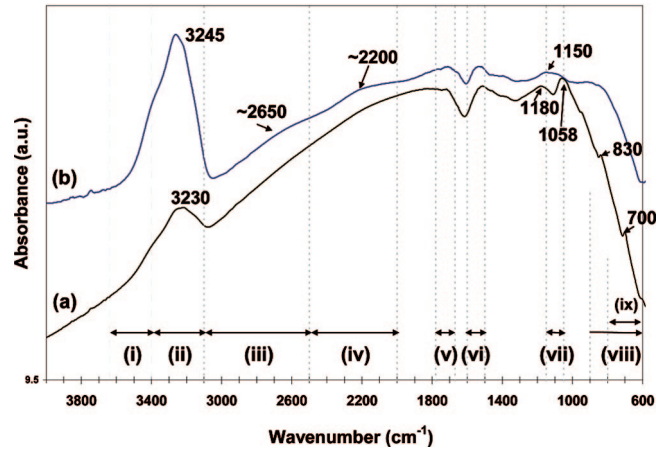

Figure 4. FTIR spectra for (a) CDC-600 and (b) CDC-1000. Regions of interest include (i) alcohol O−H stretching; (ii) adsorbed water (O−H stretching); (iii) carboxylic acids O−H stretching; (iv) triple-bond stretching; (v) carbonyl C═O stretching; (vi) aromatic stretching; (vii) alcohol C−O stretching; (viii) C−H out of plane bending; (ix) C−Cl stretch.

Surface Chemistry. FTIR was used to characterize surface chemistry, with assignment based on multiple references.[45−48] The surface chemistry of both CDC-600 and CDC-1000 is complex and heterogeneous, thus our focus in interpretation is highlighting the main features and differences between the two materials. We also restrict candidate groups to elements present from the precursor (B, C), the gases used in synthesis (Ar, Cl_2 trace H_2O, O_2), ambient air exposure (N_2, O_2), and residual IPA from the suspension. A pronounced peak at 3230−3245 cm^{-1} for both CDC-600 and CDC-1000 is likely due to water adsorption that occurred during sample transfer and exposure to ambient air (Figure 4). The high frequency shoulder on this peak is in the range of alcohols, (3400−3640 cm^{-1}) and amines (3310−3500 cm^{-1}). Amines can be ruled out as their vibrations tend to be less intense than alcohols and oxygen functional groups are much more prevalent in activated carbon materials—trace O_2 in the gases used for preparation will lead to the formation of the C−O bonds at the synthesis temperatures, as demonstrated with X-ray absorption near-edge structure spectroscopy.[29] Furthermore, any dangling bonds present after synthesis will be rapidly oxidized upon air exposure during sample handling. For CDC-1000, a broad and subtle peak at ~2650 cm^{-1} indicates carboxylic acids (2500−3100 cm^{-1}) and a broad peak at 2200 cm^{-1} indicates triple bonds (2000−2500 cm^{-1}). Both CDC-600 and CDC-1000 have vibrations associated with carbonyls (1670−1780 cm^{-1}; region 'v'), and the carbonyl vibration is more pronounced for CDC-1000. Aromatic carbons have a characteristic vibration in the range of 1500−1600 cm^{-1} (region 'vi'), and this is more pronounced in CDC-1000. However, CDC-600 has a shoulder on this aromatic peak at ~1450 cm^{-1}, an indication of aliphatic bending, a sign of greater disorder for CDC-600. Low frequency vibrations in the "fingerprint region" of FTIR show the most pronounced differences between the two samples. In the range expected for the carbon−oxygen bond for alcohols (1050−1150 cm^{-1}), CDC-600 has two features whereas CDC-1000 has one.

(45) McMurry, J., *Organic Chemistry*, 3rd ed.; Brooks/Cole Publishing Company: Pacific Grove, CA, 1992; pp 429−437.
(46) Mayo, D. W.; Miller, F. A.; Hannah, R. W., *Course Notes on the Interpretation of Infrared and Raman Spectra*; Wiley-Interscience: New York, 2004.
(47) Gomez-Serrano, V.; Acedo-Ramos, M.; Lopez-Peinado, A. J.; Valenzuela-Calahorro, C. *Fuel* **1994**, *73*, 387–395.
(48) Laboratories., S. R., *The Sadtler handbook of infrared spectra*; Simons, W. W., Ed. Sadtler Research Laboratories: 1978.

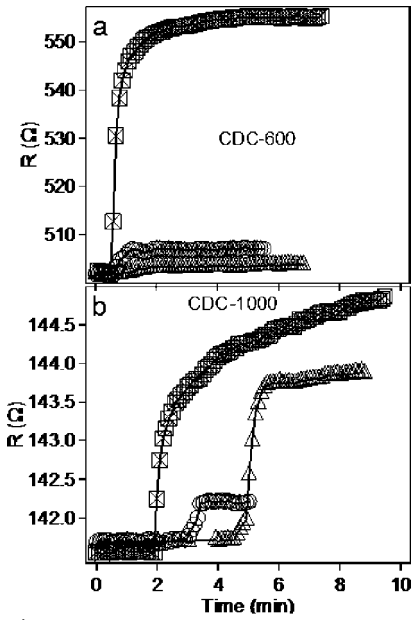

Figure 5. Initial resistive response, R, (at $P = 10$ torr) to NH_3 (squares), N_2O (circles) and room air (triangles) versus time of (a) CDC-600 and (b) CDC-1000.

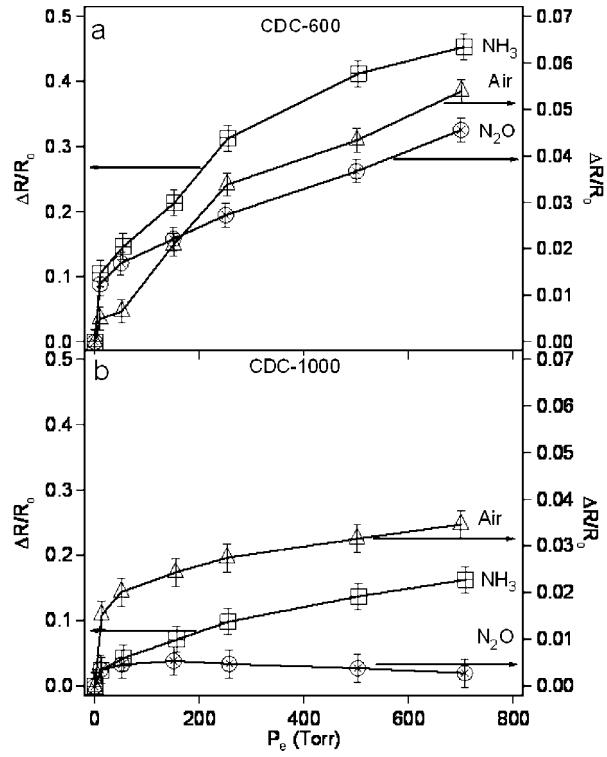

Figure 6. Response ($\Delta R/R_o$) versus equilibrium pressure (P_e) of NH_3 (squares), N_2O (circles) and room air (triangles) for (a) CDC-600 and (b) CDC-1000. The gases are plotted on two scales to accommodate large differences in response. Error bars represent one standard deviation of 2−3 measurements on different films of the same material.

With such heterogeneous samples, it is difficult to assign specifically the surrounding chemistry associated with these alcohol functionalities, but it is of note that the features in CDC-600 are much more pronounced. In the low frequency range, CDC-600 has several features not present for CDC-1000: peaks below 900 cm^{-1} can be associated with out-of-plane C−H bending and peaks in the range of 600−800 cm^{-1} are associated with C−Cl vibrations. To the best of our knowledge, FTIR has not previously been used to assess the surface chemistry of CDCs. Although X-ray absorption near-edge structure spectroscopy provided evidence for carbonyls in CDCs, which was attributed to oxygen contamination during synthesis.[29] This group mentions Cl_2 trapped during synthesis,[29,33] but makes no mention of halogenated carbons being formed.

Comparison of CDC-600 to CDC-1000. The differences between CDC-600 and CDC-1000 are subtle. Graphitic regions are starting to form at the edges of the CDC-1000 material (Figure 1), but this is a localized phenomenon and the bulk of CDC-1000 remains highly disordered, as reflected in the high D:G ratio. Structurally, the two materials have a qualitatively similar PSD, though CDC-1000 has a greater number of micropores in the range of 0.5−0.6 nm (Figure 3), and CDC-600 has a greater number of micropores in the range of ∼1−2 nm (Figure 3, inset). The large number of micropores in the range of 0.5−0.6 nm for CDC-1000 leads to increased SSA. The differences in surface chemistry are also extremely subtle, with only minor inflections for carboxylic acids and triple bonds in CDC-1000, and possible trace chlorine in CDC-600. CDC-1000 appears to have a more intense carbonyl vibration, but the functional groups within CDC-600 are more diverse with multiple peaks..

Chemical Sensing—Resistive Response. The sensors were exposed to the various gases sequentially in the following order: ambient air, N_2O, NH_3. Despite prior gas exposure, the sensor response returned to its initial resistance, R_o, with the interim treatment at 10^{-7} Torr vacuum at 100 °C, as illustrated by the absolute resistance, R, in Figure 5 at the first pressure point for each gas. At 10 Torr, the response ($\Delta R/R_o$) of CDC-600 was ∼11% for NH_3, 1% for N_2O, and ∼0.5% for room air (Figure 5a). For CDC-1000, $\Delta R/R_o$ was 2%, 0.4%, and 1%, for NH_3, N_2O, and room air, respectively (Figure 5b). The higher sensitivity to NH_3 continues at pressures up to 700 Torr for both CDC-600 and CDC-1000 (Figure 6). In the subsequent discussion, the rate of response data (i.e., Figure 5) will be distinguished from the overall response data after 30 min (i.e., Figure 6).

Discussion

Response Time Follows Kinetic Diameter, Tortuosity and Porosity. The rate of response of both CDC-600 (Figure 5a) and CDC-1000 (Figure 5b) for the various gases follows the trend predicted by kinetic diameter: the materials respond first to NH_3 (2.56 Å), second to N_2O (3.26 Å), and then to air (O_2, 3.46 Å and N_2, 3.64 Å). The effect is more pronounced for CDC-1000 than CDC-600. This is a likely effect of carbon morphology—TEM and Raman suggest CDC-1000 is more ordered. The formation of graphitic layers appear at the edges of the material and likely restricts access of probe gases to the innermost portion of the CDC material. Thus, the response for all gases is delayed in CDC-1000 relative to CDC-600. Despite greater overall micropore volume, the PSD for CDC-1000 drops rapidly in the range of 1−2 nm (Figure 2, inset) suggesting narrow channels within the CDC-1000 do not taper off, and may have limited access. The smallest probe molecule, NH_3, has a sluggish response to the tortuous CDC-1000 material and has not saturated even after 10 min (Figure 5b). The CDC-1000 and NH_3 interaction has a seeming two-phase response, suggesting there is an initial penetration into easily accessible channels followed by a secondary further penetration of the NH_3 into tightly knit, molecular size pores. The effect is less pronounced for larger gases: in CDC-1000, N_2O plateaus after ∼3.5 min and air plateaus after ∼5.5 min.

Gas Adsorption not a Predictor of Overall Resistive Response. Sensor response has been correlated to adsorption,[11] as gas-surface interaction is a prerequisite step for a change

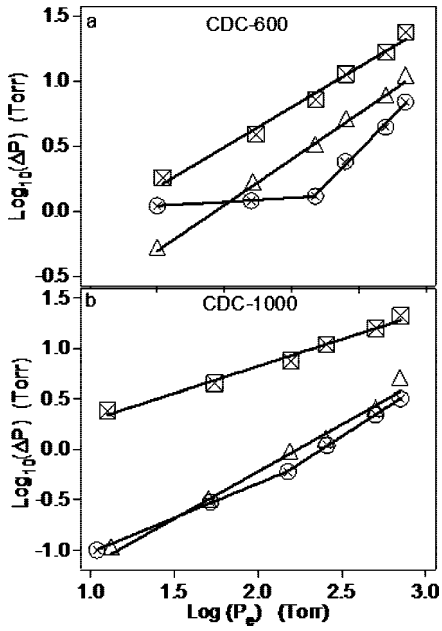

Figure 7. Log−log plot of the pressure drop upon gas exposure versus equilibrium pressure (P_e) for (a) CDC-600 and (b) CDC-1000 upon exposure to NH_3 (squares), N_2O (circles) and room air (triangles) over the entire pressure range up to 760 Torr. Pressure drop, ΔP is proportional to gas adsorbed, thus the figure is a pseudoadsorption isotherm (see text).

in the electrical properties of a chemical sensor. The superior performance of CDCs in gas adsorption[29,33] and electrochemical applications[34,49] is attributable to their high SSA and tunable porosity. The former maximizes the area available for interaction between the gas and solid, whereas the latter increases the accumulation of the probe gas at the surface due to increased surface potential. However, with all gases studied and at all pressures studied, the sensor response of CDC-600 is greater than that of CDC-1000 (Figure 6), despite the decreased SSA and micropore volume of CDC-600 relative to CDC-1000.

To consider this matter further, we consider pseudoadsorption isotherms (Figure 7). As plotted, the linear dependence on this log−log scale suggests the adsorption follows the generic Freundlich power-law adsorption isotherm. All gas-carbon combinations follow the Freundlich isotherm, except N_2O, which is discussed separately below. Comparison of the pseudo adsorption isotherm (Figure 7) to the resistive response (Figure 6) shows no correlation between adsorption and sensor response. For example, NH_3 adsorption is comparable (ratio of adsorption to CDC600 to CDC100 varies from 0.75−1.12 over the entire pressure range) in both materials, but resistive response is significantly greater for CDC-600 compared to CDC-1000 (ratio varies from 2.8−4.3 from 0−760 Torr). The other gases vary more widely between materials. The lack of correlation between the adsorption and sensor response is a likely indicator that the strength of interaction plays a role in sensor response, a factor that would not be probed by simple adsorption isotherms. The lack of correlation between SSA and sensor response is another indication that a chemical interaction (i.e., charge transfer) between the probe molecule and the sensor materials dictates sensing response in both CDC-600 and CDC-1000. In other words, the sensing response is not determined by the number of sites available for interaction (else CDC-1000 would have a greater response), but rather, the strength of interaction. The subsequent two sections consider the gases individually.

Chemical Interactions with NH_3. NH_3 is a common probe gas to assess the response of carbon-based sensors, and has led to the greatest response for both CDC-600 and CDC-1000 at all pressures. We note that the sensitivity of the CDC-600 sensor to NH_3 ($\Delta R/R_o \approx 45\%$) is large when compared to results for CNT-based sensors, which typically range from 5−13%.[2,3] The high response is without intentional oxidation, which is generally required to elicit a response to NH_3 in graphitic (hydrophobic) activated carbon and defect-free CNTs.[50] FTIR indicates oxygen groups are inherent to the CDCs, a likely result of the Cl_2 extraction process and the creation of unstable/dangling bonds that are readily oxidized.

At 300 K and 1 atm, N_2 and O_2 present in room air can be considered inert. At these conditions, the relative response to NH_3 vs room air was 8.4-fold for CDC-600 and 4.7-fold for CDC-1000 (see Figure 6). NH_3 is an electron-pair donor and is thus a Lewis base, adsorption of NH_3 implies interaction with surface acid groups of the CDC. (NH_3 adsorption is a standard test for surface acidity, as demonstrated in ref 51.) Lewis acid functional groups on CDC-1000 include carboxylic acids (2500−3100 cm^{-1}, Figure 4) and electron-deficient triple bonds (2000−2500 cm^{-1}, Figure 4). Candidate Lewis-acid functional groups on CDC-600 are not apparent from FTIR, with most detectable functional groups being of an electron-rich nature (i.e., C−Cl, C-OH). The greater response of CDC-600 to NH_3 compared to CDC-1000 must therefore be due to increased interaction with disordered carbon rather than specific electron-deficient functional groups. The functional groups attributable to disordered carbon (e.g., defects in the graphitic plane, aliphatic carbons, carbon chains, etc.) are difficult to detect in FTIR, yet still make a significant contribution to overall surface chemistry.

Interactions with N_2O. The response to N_2O was unique when compared to the other probe gases, and is considered separately. Relative to air, the N_2O response was 85% for CDC-600 and 8.1% for CDC-1000 at 760 Torr (see Figure 6). N_2O has a negative formal charge, and thus also expected to interact with Lewis-acid sites. However, N_2O has 1/10th the response of NH_3 in interacting with CDC-600 and ∼1/60th the response in interacting with CDC-1000. Furthermore, interaction of N_2O with CDC-1000 is the one gas-surface pair in which sensor response did not monotonically increase with pressure (Figure 6b). The response of CDC-1000 increased initially with N_2O pressure, then began to decline at $\sim P = 150$ Torr. Also, N_2O did not follow the generic Freundlich power-law adsorption isotherm (Figure 7), an indication of activated adsorption, slow adsorption equilibrium, or a sign of chemical reaction. The latter would be unexpected at room temperature without catalyst.

Summary and Conclusions

This work explores carbide derived carbons as room temperature gas sensors. Both the response time and overall response of the sensors were related to the carbon morphology, which can be altered by varying the CDC preparation conditions. Specifically, higher CDC preparation temperatures led to the formation of external graphitic layers that impeded the sensor response time. Gas adsorption, including both standard measurements of surface area and porosity (using N_2 BET and DFT analysis) and quantification of the direct adsorption of the probe gas, did not follow the trends in the sensor response, suggesting charge transfer between the probe gas and the CDC led to the resistive response. CDCs provide a strong response to NH_3 without additional surface modification or chemical functionalization. Sensing materials with increased carbon order had a decreased resistive response, despite more sites for interaction. The results suggest the probe

(49) Chmiola, J.; Yushin, G.; Dash, R.; Gogotsi, Y. *J. Power Sources* **2006**, *158*, 765–772.

gases interact with disordered carbon (e.g., defects in the graphitic plane, aliphatic carbons, carbon chains, etc.) which do not have a strong FTIR fingerprint but are reflected in the Raman spectroscopy and TEM characterization.

Acknowledgment. The work was funded through the American Chemical Society Petroleum Research Fund (43431-G10), a Deike Research Grant, and the Pennsylvania State University. The authors gratefully acknowledge Drs. Joe Kulik and Humberto Gutierrez for performing the TEM analysis, Xiaoming Liu for FTIR guidance, and John Badding for Raman collaboration.

LA800465E

(50) Paulson, O.; Pugh, R. J. *Langmuir* **1996**, *12*, 4808–4813.
(51) Kim, B. J.; Park, S. J. *J. Colloid Interface Sci.* **2007**, *311*, 311–314.